Chinese Chemical Letters 34 (2023) 108194

Contents lists available at ScienceDirect

Chinese Chemical Letters

journal homepage: www.elsevier.com/locate/cclet

From surface loading to precise confinement of polyoxometalates for electrochemical energy storage

Chongji Wang[a,b], Yanhui Song[c], Wenhua Cong[a], Yuanyuan Yan[a], Meiling Wang[a,b,*], Jiadong Zhou[b,*]

[a] College of Materials Science and Engineering, Taiyuan University of Technology, Taiyuan 030024, China
[b] Centre for Quantum Physics, Key Laboratory of Advanced Optoelectronic Quantum Architecture and Measurement (MOE), School of Physics, Beijing Institute of Technology, Beijing 100081, China
[c] Instrumental Analysis Center, Taiyuan University of Technology, Taiyuan 030024, China

ARTICLE INFO

Article history:
Received 14 October 2022
Revised 27 January 2023
Accepted 5 February 2023
Available online 8 February 2023

Keywords:
Polyoxometalates
Non-confinement
Confinement
Electrochemical energy storage
Supercapacitor
Battery

ABSTRACT

Because of abundant redox activity, broad tunability, and specific atomic structure, polyoxometalates (POMs or POM) clusters have attracted burgeoning interests in electrochemical especially energy storage fields. Nevertheless, due to the high solubility and fully oxidized state, they often suffer from electrically insulation as well as chemical and electrochemical instability. Traditional noncovalent loading or covalent grafting of POMs on conductive substrates have been successfully performed to overcome this problem. However, severe shedding or agglomeration of POMs arising from weak interactions with substrates or excessive entrapment or weak destruction in conductive supports cause significantly reduced availability and stability. To this end, precise confinement of POMs into conductive supports has been tried to improve their dispersibility and stability. Herein, recent progress of POMs from surface loading to precise confinement in the electrochemistry energy storage field is reviewed. Firstly, we illustrate the typical non-confinement methods (*viz.* covalent and non-covalent) for supported POMs in energy storage applications. Secondly, different strategies for precise confinement of POMs in organic and inorganic materials for related applications are also discussed. Finally, future research directions and opportunities for confined POMs, and derived ultrafine nanostructures are also proposed. This review seeks to point out future research directions of supported POMs in the electrochemistry-related fields.

1. Introduction

With the rapid development of technology and economy, increasing demand and limited resources are gradually conflicting. Among the large numbers of energy storage technologies, electrochemical energy storage devices such as lithium-ions batteries (LIBs) [1] and super-capacitors (SCs) [2,3] have become the important component for next-generation integrated electronics. Generally, electrode materials with excellent activity and stability are fundamental parts for building electrochemical energy storage devices [4,5]. Therefore, exploring selective and efficient electrode materials has become the most important task [6–8]. The search for earth-abundant, highly-efficient, and environmentally friendly materials has brought polyoxometalates (POMs) to the forefront as active material for high-performance energy storage devices [9–11] owing to their rich structure, and electronic sponge properties [12–14].

Specifically, POMs are an exceptional group of metal oxygen cluster formed by early transition metals of highest oxidation state [15,16] with reversible multi electron transfer properties and good chemical stabilities [14,17]. Its thermal and chemical stability can be adjusted and its structural size can also be turned by changing the composition [18]. According to their structures, POMs can be divided into Keggin-type, Dawson type, Anderson type, Silverton type, Lindqvist type and Waugh type [19]. Among them, Keggin-type POMs with a size of about 1 nm, such as phosphomolybdic acid (PMo_{12}) and phosphotungstic acid (PW_{12}), have been widely studied due to their most stable structures [20–22]. Unfortunately, electrically insulating [23] and high solubility of POMs largely hinder their application [24]. Recently, noncovalent loading [25–27] or covalent grafting of POMs on supports [28–30] have been applied to loading POMs for electrochemical energy storage applications.

* Corresponding authors.
E-mail addresses: wangmeiling@tyut.edu.cn (M. Wang), jdzhou@bit.edu.cn (J. Zhou).

https://doi.org/10.1016/j.cclet.2023.108194
1001-8417/

Each of these linking methods will be explained in detail later in this review. Despite significant developments in improving POMs behavior by anchoring onto the conductive substrate, there are still leaching or agglomeration problems of POMs arising from weak interaction or over-embedding in substrates. This results in low utilization and reduced active site exposure of POMs [25,26,31,32]. To avoid these shortcomings, many organic nano porous materials such as metal–organic frameworks (MOFs), covalent organic frameworks (COFs) and a rational designed amorphous polymer hydrogel with a supermolecule cage [33] have been selected to confine single POM molecule to resist sintering [34–39]. More recently, precise confinement of Keggin-type POM molecules in porous carbon with certain diameters or a unique porous carbon with a unimodal super-micropore also have been reported [40].

Considering the above background, the present progress report provides the development process of POMs in common electrochemical energy storage applications from surface loading to precise confinement. The schematic diagram shown in Fig. 1 illustrates the main development history of supported POMs broadly [12,25,33,41–50]. The first purpose of this review is to illustrate typical non-confinement approaches (*i.e.*, covalent, and non-covalent) for supported POMs in the field of electrochemistry energy storage. Second, we mainly focus on elucidating state-of-the-art strategies to confine individual POM molecules in organic and inorganic materials. The report presented herein also suggest more simple confinement strategies or substrates to improve the dispersibility and stability of POMs. These efforts can ultimately enhance the single POM molecule dispersibility to induce their intrinsic activity for advanced electrochemical energy storage systems. Finally, a brief overview of future pathways for confined POMs, and correspondingly derived ultrafine nanostructures as well as POMs-supported single-atom catalyst is provided, which sheds some light on the synthesis of ultrasmall non-precious metal nanostructures for electrocatalysis fields.

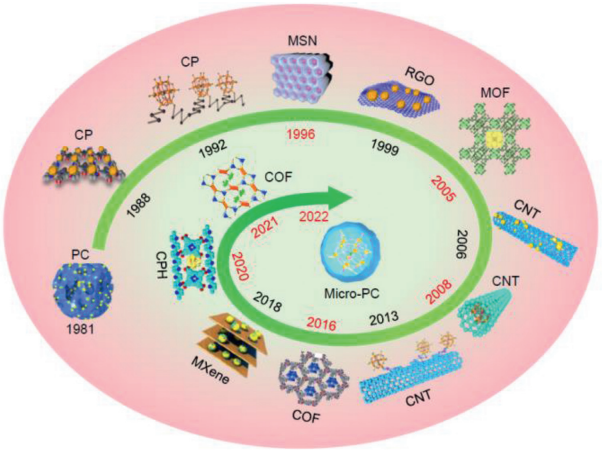

Fig. 1. A brief timeline showing the history of development of supported POMs. Inset images: Porous carbon (PC) supported POM (1981); Polymer supported POM (1988) [41]. Reproduced with permission [160]. Copyright 2019, Elsevier. POM-polymer by covalent linking (1992) [42]; POMs confined in zeolites (1996) [43]; Graphene supported POM (1999) [44]; POMs confined in metal–organic frameworks (MOFs) (2005) [45]. Reproduced with permission [150]. Copyright 2018, Royal Society of Chemistry. Carbon nanotube (CNT) supported POM (2006) [46]; POMs confined in CNT (2008) [47]; POM-CNT by covalent linking (2013) [48]; POMs confined in covalent organic frameworks (COF) (2016). Reproduced with permission [49]. Copyright 2016, American Chemical Society. MXene supported POM (2018) [25]; POMs confined in polymer hydrogel (2020). Reproduced with permission [33]. Copyright 2020, Royal Society of Chemistry. POMs confined in COF by covalent linking (2021). Reproduced with permission [12]. Copyright 2022, American Chemical Society. POMs confined in PC of unimodal super-micropore (2022). Reproduced with permission [40]. Copyright 2022, John Wiley & Sons, Inc.

2. Structure and properties of POMs

Based on their composition, POMs can be divided into isopolyacids (IPA) and heteropolyacids (HPA) [50]. In comparison with IPA, in addition to transition metal ions (complementary atoms) and oxide ions, HPA also contains one or more elements in the normal oxidation state (heteroatoms) from the p, d or f regions of the periodic table [51]. Although these heteroatoms account for a small proportion of the number of complementary atoms in the structure of HPA, the structure, composition and properties of HPA vary greatly from one heteroatom to another. By changing the type and proportion of heteroatoms and complementary atoms, HPA shows novel electrochemical performance than the original structure [52]. Therefore, this paragraph introduces POMs by analyzing HPA. HPA, as a protonated metal oxidation cluster, can be expressed as $H_nA_xM_yO_z$, where: A stands for heteroatoms, such as Si^{IV} and P^{V}; M represents supplemental metal atoms, usually Mo^{VI}, W^{VI} [53]. In the crystal structure of HPA, the transition metal and oxygen atoms are linked to form oxide crystals through sharing oxygen atoms [54,55]. Besides, the heteroatoms are also connected to each other by sharing adjacent oxygen atoms with metal atoms [56]. As shown in Fig. 2, according to the ratio of metal atoms to heteroatoms, HPA can be divided into Keggin and Silverton types (1:12), Dawson and Waugh types (1:9), as well as Anderson (1:6) and Lindqvist types (6:19). Meanwhile, it can be divided into tertiary structures by its stacking behavior. The primary structure is the six structures mentioned above. While the one consisting of the above molecular structures and bound water or other molecules in solid state form is denoted as secondary structure. For the tertiary structure, it refers to the particles formed after the stacking and assembly of HPA, including particle size, and pore structure, which has the greatest influence on the properties of HPA [20].

Besides, the composition and structure of HPA brings it unique properties: (1) The structure is changeable and soluble in oxygen-containing solvents; (2) Stable redox valence states of transition metals enable them adjusted potential and composition, as well as good redox properties [57]; (3) Unique basic polyanions acting as ligands and supports for metals and organometals makes HPA malleable [58]; (4) The controllable tertiary structure and bulk behavior endow HPA with good thermal stability and large molecular size. Specially, Keggin-type POMs exhibit excellent electrochemical stability owing to their more stable structure, which can undergo reversible multiple protons/electrons transfer while maintain stable structure [59]. Herein, Keggin-type POMs is taken as an example to illustrate its redox reaction [60]:

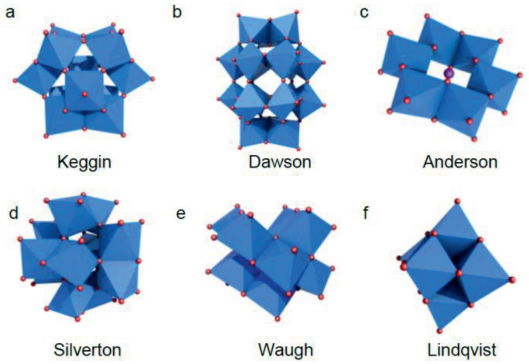

Fig. 2. Six fundamental POM structures. By analyzing the ratio of addenda atoms to hetero atoms, POMs can be divided into: Keggin and Silverton type (1:12), Dawson and Waugh type (1:9), Anderson type (1:6), Lindqvist type (6:19), respectively.

Positive:

$$Co^{II}W_{12}O_{40}^{6-} \leftrightarrow Co^{III}W_{12}O_{40}^{5-} + e^- \quad (1)$$

$$\Phi_0 = 1.103 \text{ V } vs. \text{ SHE}$$

Negative:

$$CoW_{12}O_{40}^{6-} + 2e^- + 2H^+ \leftrightarrow H_2CoW_{12}O_{40}^{6-} \quad (2)$$

$$\Phi_0 = -0.074 \text{ V } vs. \text{ SHE}$$

$$H_2CoW_{12}O_{40}^{6-} + 2e^- + 2H^+ \leftrightarrow H_4CoW_{12}O_{40}^{6-} \quad (3)$$

$$\Phi_0 = -0.191 \text{ V } vs. \text{ SHE}$$

The whole reaction is concentrated on the crystal surface because the slow reaction of electron with oxygen atoms is a rate-controlled step [61]. So, the specific surface area of POMs also has a great influence on its electrochemical performance. Additionally, its high solubility in polar solutions severely limits its application [62]. To sum up, uniform dispersion of POMs onto/with conductive substrate is meaningful for its applications.

POMs were first promoted as molecular cluster batteries by Awaga and Yoshikawa *et al*. in 2012 [63]. In POMs-based batteries, the reversible uptake-release of Li^+ or Na^+ in POMs and accompanied redox reactions make POMs behave like an "electron/ion sponge" in batteries and supercapacitors (SCs). Generally, SCs contains electrical double-layer capacitor (EDLC) and pseudo capacitor. During the charging/discharging processes, only physical electrostatic charge accumulates in the EDLC, while fast redox reactions also occur in pseudo capacitor. So, owing to the "semipermeable molecular capacitor" redox behaviors and the high stability of the redox states, POMs can be applied as promising candidates for batteries (*e.g*., LIBs and sodium-ion batteries (NIBs)) and SCs. The application of POMs in the field of LIBs, NIBs and SCs is mainly based on its multi-electron redox characteristics, and the focus of this review is to summarize the advance of POM from simple loading to confinement for the mainstream energy storage applications. In order to analyze the evolution of the supported POMs, an overview will be given from the perspective of the loading strategy (Fig. 3).

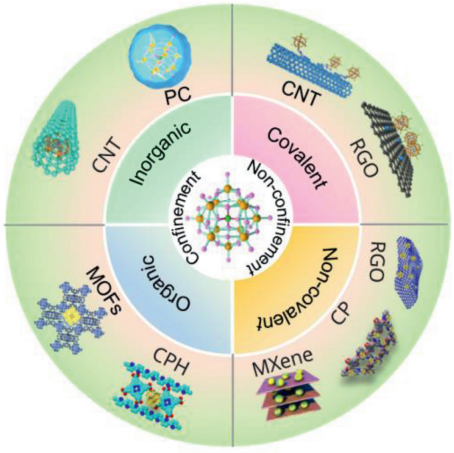

Fig. 3. Surface loading and precise confinement strategies of POMs in this review for electrochemical energy storage.

3. Strategies for supported POMs in batteries and SCs

Note that their solubility in water and organic solvents and poor conductivity limits the application of utilizing POMs as electrode materials because they cannot readily form insoluble membranes or films on their own. POM–conductive supports is a promising strategy to solve the poor film-forming and low intrinsic electronic conductivity problems [64].

To meet the requirements of high energy/power densities and long cycle life of batteries or SCs, POM molecules should maintain a stable multi-electron transfer state during charging/discharging process. Moreover, in order to maximize the performance of POMs, there are many considerations in the substrate selection and designing. First, the substrate should not only offer stability and recyclability [65], but also provides high surface area [66] and conductivity [67,68]. This can endow the composite with good cyclic performance and a high loading of POMs. Second, it is desirable for the substrate to retain the maximum number of active sites of POMs for its intimate contact with the chemical environment. Closer contact with the substrate and exposure to more active sites can stimulate its intrinsic activity. Lastly, electron transfer is preferred to enhance their activity through charge/carrier synergy [69]. This requires good conductivity of the substrate to speed up electron/ion transport. According to the combination forms of POMs with the substrate, the strategies can be divided into confinement and non-confinement. Note that the so-called non-confinement type refers to the way that POMs combine with the substrate in the form of agglomerated particles or clusters by covalent and non-covalent forms. While the confinement means that POM is confined in the pore of nano porous materials (including crystalline and amorphous materials) in the single molecule form.

3.1. Non-confinement

For non-confinement-related system, various intermolecular forces are involved between POMs and substrate (such as polymer, porous carbon, graphene (or RGO), CNT, MXene), including non-covalent, and covalent interactions which will be discussed in this chapter by some examples.

3.1.1. Non-covalent interaction

Polymer supported POMs: Since 1977, Heeger *et al*. discovered the electronic conductivity of doped conjugated polymers, the research on organic polymers has obtained wide attention [70]. This polymer conducts electricity mainly through the delocalized electrons of the main chain, which not only brings efficient capacitive performance, but also gives it the basis for combining with other materials [71,72]. They are often used as substrate materials owing to their low weight and ductile nature [73,74]. It is usually used to support POMs by physical cross-linking and electrostatic interaction through its rich functional groups or positive properties [75–78]. Note that the polymer is usually further treated before supporting POMs owing to its poor electrical conductivity. For example, Han *et al*. have used micro/nanostructured polypyrrole (PPy) by "soft-template" methods supporting POMs, which provides improved electrochemical performance than PPy with irregular morphology due to the reduction of electron diffusion resistance [79].

Porous carbon (PC) supported POMs: Besides polymers, "carbon materials" are also widely studied as substrate materials [80]. The "carbon material" here refers to sp^2-hybridized carbon of well-defined nano-structures [81–83]. It has been found that there is a strong chemisorption between POMs and carbon materials [84]. Since 1981, Yusuke successfully loaded PW_{12} and SiW_{12} onto commercial activated carbon (AC) by impregnation method [85]. PW_{12} adsorbed onto AC as electrode materials was applied to SCs

by V. Ruiz., which stimulated the development of the field [86]. This method introduces Faraday behavior into the hybrid material, which not only expands the voltage window of the SCs in acidic liquid electrolyte to 1.6 V, but also provides a large capacitance of 254 F/g. However, the pore structure of commercial AC has not been fully utilized, and the supported POMs is still non-uniform [87]. Later, Pablo Palomino group has attempted to adjust the pore size of AC to further improve the capacitance of AC-supported POMs. Although this report improves the dispersion of POMs by adjusting the pore size, a large amount of leaching or aggregation of POMs still occurs due to the existence of many mesopores [88]. Therefore, the size control of the substrate hole is very important.

Graphene supported POMs: As a popular carbon nanomaterial, graphene is essentially a two-dimensional sheet of sp^2-hybridized carbon [89]. Its long-range π-conjugated structure endows it with excellent chemical/physical properties, and its unique surface structure and large specific surface area also make it a hot research topic for substrate materials [90,91]. Corresponding SCs with excellent performance were first prepared by Kunio Awaga's team through the natural adsorption of POMs on graphene (Fig. 4a) [92], where PMo_{12} agglomerates into 2–3 nm clusters (Fig. 4b). To increase the interaction between the two, Bao-Hang Han group inserted POMs into graphene interlayers to assemble a three-dimensional porous structure [93]. This structure connected by anion-π non-covalent interactions involves efficient electron transfer, showing a large specific surface area (680 m^2/g). The POMs were not observed by typical transmission electron microscope (TEM), which may be attributed to uniform distribution of POMs and it is expected to be further studied by advanced characterization techniques.

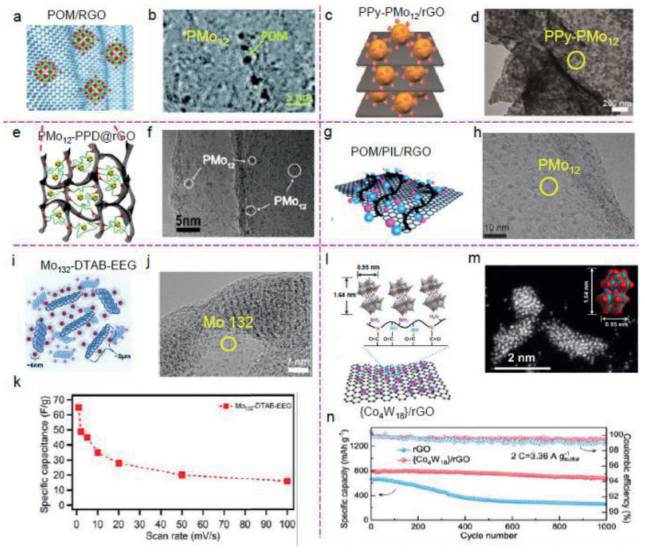

Fig. 4. Schematic of non-covalent strategies for POM-graphene. (a, b) Natural adsorption of POM on graphene, and corresponding TEM image. Reproduced with permission [92]. Copyright 2014, Royal Society of Chemistry. (c, d) Grafting of PPy-PMo_{12} by electrostatic interaction on RGO, and corresponding TEM image of PPy-PMo_{12}/rGO. Reproduced with permission [95]. Copyright 2015, Royal Society of Chemistry. (e, f) Covalently grafting of PPD-POM obtained by electrostatic interaction on RGO, and corresponding TEM image of PMO_{12}-PPD@rGO. Reproduced with permission [96]. Copyright 2020, Royal Society of Chemistry. (g, h) Electrostatic bridging POM on RGO by PIL, and corresponding TEM image of POM/PIL/RGO. Reproduced with permission [97]. Copyright 2014, Wiley-VCH. (i-k) Van der Waals forces grafting Mo_{132}-DTAB obtained by electrostatic interaction on graphene, and corresponding TEM image of Mo_{132}-DTAB-EEG, respectively. Reproduced with permission [98]. Copyright 2019, Elsevier. (l-n) Electrostatic bridging Co_4W_{18} on rGO by PEI and corresponding SEM image, as well as cycling stability of Co_4W_{18}-based Li-S batteries. Reproduced with permission [99]. Copyright 2022, Nature Publishing Group.

Since POMs is negatively charged, several organic polycations and molecules have been developed to induce positive charges on the carbon surface to adsorb POMs [94]. For example, Professor Lan's group reported the synthesis of novel PPy–POM/rGO *via* a PMo_{12}-mediated one-pot redox strategy (Fig. 4c). In which POMs acts as the oxidant of pyrrole, then it was connected to the RGO layer by PPy through electrostatic interaction, forming a negative-positive-negative electrostatic interaction structure [95]. Although the designed SC exhibits good rate capability, and mechanical stability, this strategy still fails to address the ever-present agglomeration problem (Fig. 4d), and poor stability [92]. Similarly, the conductive polymer of polyp-phenylenediamine can also serve as a bridging agent. For example, Li's team covalently grafted poly(*p*-phenylenediamine) (PPD)-PMo_{12} on three-dimensional RGO structure (PPD-PMo_{12}@rGO) (Fig. 4e) [96]. The covalent interaction between the "bridge" PPD and RGO enables better electrons transfer from the PMo_{12} to the RGO. Although this hybrid exhibits a high specific capacitance (790 F/g at 1 mV/s) for SC, the agglomeration of PMo_{12} still occur, as nanoparticles larger than 1 nm were observed by TEM (Fig. 4f).

To further enhance the interaction with graphene, Lee *et al.* use polyconic liquid (PIL) as bridging agent, where PMo_{12} and graphene are also firmly connected by negative-positive-negative electrostatic interaction (Fig. 4g). The composite delivers a high capacitance density (408 F/g at 0.5 A/g) for SCs due to the improved dispersibility of PMo_{12} as shown in Fig. 4h [97]. Later, Samori *et al.* produced a novel architecture, in which Keplerate-type POM (Mo_{132}) functionalized with surfactant of DTAB was linked to graphene (Figs. 4i and j) [98]. However, the low loading, a certain non-unimolecular connected with the introduction of surfactants lead the reduction of electrical conductivity, causing the decreased electrochemical performance (Fig. 4k). Surprisingly, in early 2022, with the electrostatic assembly approach, the positively charged poly(ethyleneimine) (PEI) linker was used to anchor monodisperse $Co_4(PW_9O_{34})_2^{10-}$ (Co_4W_{18}) clusters on the RGO (Fig. 4l). It can be seen from the Fig. 4m, single molecular framework of Co_4W_{18} were uniformly loaded onto the RGO substrates, which delivers long-term Li-S battery cycling performance with a capacity fading of 0.015% per cycle after 1000 cycles at 2 C (Fig. 4n) [99]. Obviously, the introduction of bridging agent is necessary to enhance the stability and dispersion of the clusters. Obviously, non-covalent linking of POMs with RGO is realized by using a positively charged polymer or PIL as a bridge.

Carbon nanotube supported POMs: Carbon nanotubes (CNTs), as a conductive carbon material inherited from graphene, also have unique thermal and electronic properties, making them a popular choice for the substrate materials [100]. Although it is lack of pores, its surface defects usually bring abundant nucleation sites for stabilization nanoparticle [101,102]. Initially, the researchers load POMs onto CNT through electron transfer from the POM to the CNT by ultrasound, which was applicated in molecular cluster batteries (Fig. 5a), however, similar agglomeration was still observed as shown in Fig. 5b [103]. Subsequently, the electrostatic bridging strategy is also used for loading POMs on the surface of carbon nanotubes (CNTs). For example, Toma *et al.* decorated CNT with organic $[(CH_3(CH_2)_3)_4N]^+$ (TBA) cations bridge to support anionic $[PV_2Mo_{10}O_{40}]^{5-}$ anions, resulting in a relatively uniform dispersion of PV_2Mo_{10} on CNT (Figs. 5c and d). In the SWCNT-TBA-PV_2Mo_{10} nanohybrid material, TBA-PV_2Mo_{10} provides redox activity benefiting from the high electrical conductivity and high double-layer capacitance of the SWCNTs, bringing improved energy and power density for SCs [26]. However, in addition to introducing non-conductive molecules, this electrostatic bonding strategy often brings unnecessary electron transfer and re-

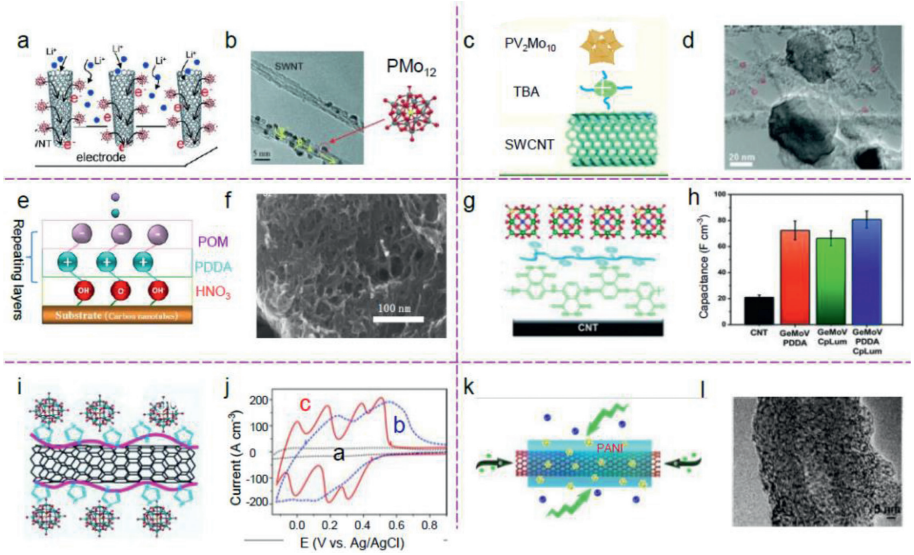

Fig. 5. Schematic of non-covalent strategies for POM-CNT. (a) $TBA_3[PMo_{12}O_{40}]$ molecules adsorbed onto the surfaces of CNT by suction filtration. (b) TEM image of the $TBA_3[PMo_{12}O_{40}]$/CNT. Reproduced with permission [103]. Copyright 2011, John Wiley and Sons Ltd. (c) Electrostatic capture of PV_2Mo_{10} clusters by organic TBA cations on CNT. (d) TEM image of SWCNT-TBA-PV_2Mo_{10} nanohybrids. Reproduced with permission [26]. Copyright 2015, Royal Society of Chemistry. (e) Electrostatic bridging of POM on CNT by non-conductive polymer PDDA. (f) SEM image of film from $SiMo_{12}$/PDDA/PMo_{12}/CNT [105]. Reproduced with permission [105]. Copyright 2011, Elsevier. (g) Layer-by-layer assembly of GeMoV-polyluminol composite by electrostatic interaction. (h) Capacitance comparison of bare CNTs and CNT modified with different assemble system. Reproduced with permission [106]. Copyright 2020, Royal Society of Chemistry. (i) Electrostatic linking of POM on CNT by IL. (j) CV comparison of bare CNT and modified CNT electrodes at 1000 mV/s. Reproduced with permission [109]. Copyright 2016, American Chemical Society. (k) Schematic representation of the PMo_{12}/PANI/MWNTs nanocomposite. (l) TEM image of PMo_{12}/PANI/MWNTs. Reproduced with permission [110]. Copyright 2017, Elsevier.

duces the structural stability of POMs, thus limiting its practical application in electrochemistry [63,104]. In order to avoid leaching, Keryn Lian's team also used poly(dimethyldiallylammonium) (PDDA) as bridge to connect POM with CNT (Fig. 5e). Later, based on layer-by-layer (LBL) method, CNTs were successfully modified with inorganic/organic composites as shown in Fig. 5f. By superimposing layers of different pseudocapacitive $SiMo_{12}$ and PMo_{12}, the POMs exhibited continuous overlapped oxidation/reduction reactions and achieved an up to fourfold increase in area specific capacitance when compared with the double layer capacitance of bare MWCNTs. Nevertheless, electrochemically inactive PDDA induced additional resistance [105]. Alternatively, Keryn Lian *et al.* also fabricated an GeMoV-polyluminol hybrid materials for SCs by using polyluminol (CpLum) and PDDA as organic layers and Keggin-type POMs as inorganic layer (Fig. 5g). It was found that the volumetric capacitance exceeds the individual organic molecule anchored GeMoV electrodes owing to co-contribution of PDDA (attracting more GeMoV through electrostatic interactions) and CpLum layer (improving conductivity) (Fig. 5h) [106]. Moreover, another POM/CNT nanohybrids were also assembled through LBL self-assembly by V. Jawale *et al.* [107] and Bajwa [108] for SCs. Owing to the poor electrical conductivity of polymers. By learning from the early strategy, Keryn Lian *et al.* further proposed using ionic liquids (IL) to connect them, and it has been reported that such composites show better capacitor performance than that with polymer as bridges (Figs. 5i and j) [109]. Similarly, polyaniline (PANI) was also applied as bridge to connect PMo_{12} and CNT (Fig. 5k). As shown in Fig. 5l, the PMo_{12} clusters are attached electrostatically to the PANI/MWNTs composite material. The electrochemical performance of the PMo_{12}/PANI/MWNTs nanocomposite as anode material for LIBs shows an overall discharge capacity of 1000 mAh/g for 100 cycles at a current density of 0.5 mA/cm^2 [110]. Clearly, all strategies use intermediate molecules (*e.g.*, organic cations, IL/PIL, polymer) as "bridges" to connect POMs to CNT or RGO in a negative-positive-negative manner. However, the agglomeration problem of POM has not been solved due to the limited and non-directional electrostatic interactions. It can be speculated that these strategies also apply to other substrates.

MXene supported POMs: Recently, like graphene, MXene obtained by etching the MAX phase in 2011 [111] has attracted much attention owing to its layered two-dimensional structure, excellent electrical conductivity, and high theoretical capacitance [112–114]. In recently years, the research on the combination of MXene and POMs is also increasing. For example, Mo and Fe-based POMs (MF POM) were in situ anchored on MXene by Hao *et al.* (Fig. 6a) [115]. The obtained composites can provide good performance thanks to the synergistic effect of POMs and MXene. This strategy avoids the introduction of third-party materials. However, the problem of embedding POMs into MXene layers and poor conductivity problems remain unsolved (Fig. 6b). The Li/Na storage performance can further be improved (Fig. 6c). Despite the successful combination of MXene and POM, there is still room for improvement, such as the introduction of bridges to improve their conductivity [116]. More recently, Xu *et al.* also supported POMs on MXene through interfacial linker PIL with the impregnation method (Fig. 6d). Clearly, the electrostatic interactions and anion exchange of PIL not only stabilize POMs on the MXene, but also overcome the stacking of MXene layers and improve the electron conductivity. However, the supported POMs also exhibited poor dispersion (Fig. 6e), despite showing higher stability for SCs compared to POM-MXene (Fig. 6f) [25]. In addition to PIL, MXene/POMs hybrid was also synthesized by embedding the POMs with a PPy layer [117] or amino-(polyethylene glycol)$_{2000}$ (NH_2-PEG_{2000}) [116] for sensing applications.

Similarly, Zhu *et al.* also provided new improvement on POM/MXene composites by compounding PW_{12}, MXene and PC, which shows more homogenous distribution of PW_{12} clusters. In the composite, PW_{12} and PC were compounded into the interlayer of MXene, with no direct physical contact and electron transport between PW_{12} and MXene [118]. Nano-dispersion of POMs facilitates charge storage through surface capacitive processes (91% at 2 mV/s) for SCs. In early 2022, a SiW_{12}-based coordination polymer $Zn(itmb)_3H_2OH_2SiW_{12}O_{40}{\cdot}5H_2O$ with two water-assisted pro-

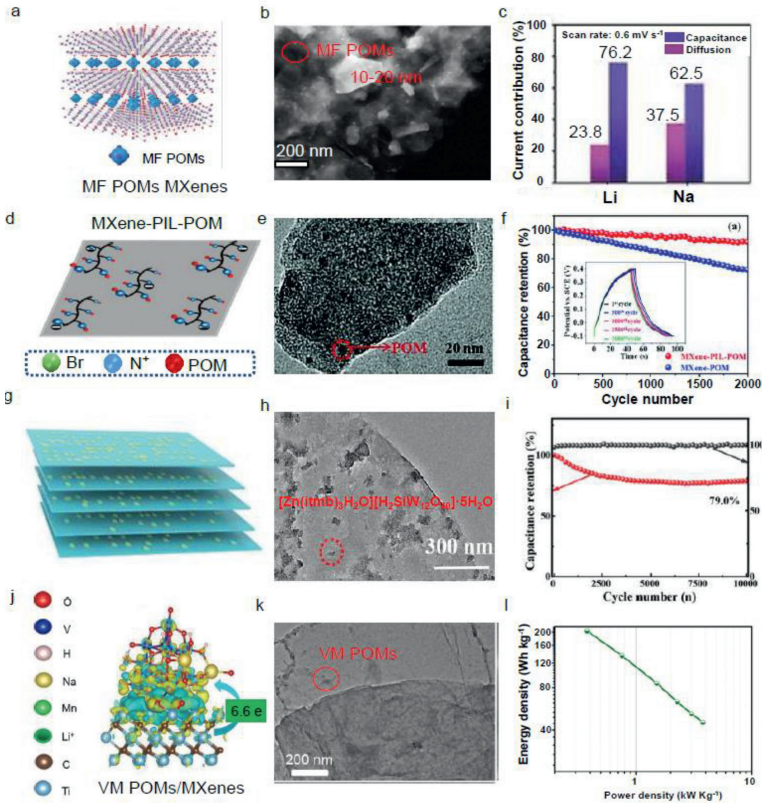

Fig. 6. Schematic of non-covalent strategies for POM-MXene. (a) *In situ* growth of MF POM/MXene composite by coordination. (b) TEM image of MF POM/MXene. (c) Boosted lithium/sodium contribution by bonding polyoxometalate on MXene nanosheets. Reproduced with permission [115]. Copyright 2021, Wiley-VCH. (d) Electrostatic linking POM on MXene by poly ionic liquid. (e) STEM image of MXene-PIL-POM. (f) Lifetimes comparison. Reproduced with permission [25]. Copyright 2018, Royal Society of Chemistry. (g) POM-based coordination polymer $[Zn(itmb)_3H_2O][H_2SiW_{12}O_{40}]\cdot 5H_2O$ loaded on MXene by filiation. (h) TEM image of $[Zn(itmb)_3H_2O][H_2SiW_{12}O_{40}]\cdot 5H_2O$/MXene. (i) Cycling stability of the corresponding device (20 A/g). Reproduced with permission [119]. Copyright 2022, Wiley-VCH. (j) Charge density distribution of VM POMs/MXene fabricated by freeze-drying the mixture of POMs and MXene. (k) TEM mage of VM POMs/MXene. (l) Ragone plot of VM POMs/MXene-based rate-capable device. Reproduced with permission [120]. Copyright 2022, Springer.

ton channels interlayered into the MXene spacers was designed for the SCs application (Fig. 6g). As shown in Fig. 6h, the SiW_{12}-based coordination polymer is evenly distributed on the surface of the ultrathin MXene nanosheets. Moreover, the supercapacitor device shows desirable capacity retention of 79.0% (10,000 cycles, 20 A/g), suggesting good stability (Fig. 6i) [119]. More recently, a new local electric field concept was firstly utilized to the POM-based electrode material for lithium batteries, where 2D VM POM nanoplates connected with MXene by simply mixing two dispersions. As shown in Fig. 6j, the fast charge transfer occurs at the interfaces of support and VM POMs. The TEM image of VM POMs/MXene composites reflects transparent sheet, indicating the ultrathin thickness of MXene, where the VM POMs are uniformly decorated onto (Fig. 6k). Moreover, a high energy density 195.5 Wh/kg at power density of 380 W/kg is achieved when applied for SCs (Fig. 6l) [120]. Obviously, 2D MXene is also good choice of substrates because of their large surface facilitating the formation of robust interfaces with POMs. The vigorous synergistic effects can be essentially harvested, especially with strong chemical bonding formed between them. Such a combining can essentially harvest the rich redox-activity of POMs and metallic conductivity of MXene.

3.1.2. Covalent interaction

By non-covalent bonding with substrate, the composite combines the merits of each component. However, due to the non-directivity of the force, POMs molecular tend to aggregation and the overall stability is still unresolved [121]. The covalent bonding is different from the non-covalent modification process for supported POMs because it involves a more highly stable link between POMs and substrates [122]. Note that although covalent-linking can bring more excellent stability of supported POMs, just as every coin has two sides, the direct covalent-linking POM onto the substrate also may destroy the structure of POMs to a certain extent. Besides, covalent grafting rate is not so high.

POMs-polymer by covalent linking: As we known, when POMs are introduced into the polymer substrate, it is vulnerable to leaching, which further limits its inherent capacitance [28,73]. In comparison with electrostatic interactions and hydrogen bonding, covalent bonding is the most stable [123]. Indeed, incorporating POMs into the side chains [124] and main-chains [123] of traditional polymers *via* covalent-bond have been developed. For example, Lu *et al.* combined molybdate molecules with poly(phenylene acetylene) by forming metal-nitrogen bonds, forming a structure with multiple polymers linking a molybdate molecule [123]. Alshehri *et al.* also creatively used electric polymerization to covalently connect molybdate to PPy chain with imine bond, showing promising electronic, optical, and electrochemical properties. It showed the specific capacitance the polymer films are enhanced owing to the modifying of the PPy film by POMs, and a substantial additional faradaic contribution is introduced through the POM redox processes [125].

POMs-RGO by covalent linking: Recently, a “point linking” method is also presented to covalently link POMs with graphene [126]. For example, Professor Lan *et al.* applied a “point-linking” strategy to anchor $MnMo_6$–$2NH_2$ on graphene surfaces with amino groups as bridges (Fig. 7a) [127]. In this system, the covalently connected $MnMo_6$–$2NH_2$–GO ultrathin nanosheets is as thin as

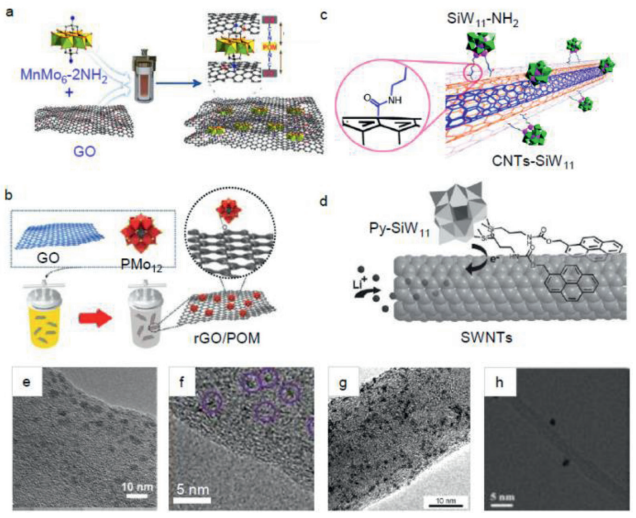

Fig. 7. Schematic of supported POMs with covalent bonding interaction. (a) $MnMo_6$ anchored on graphene surfaces through Mo–N bond. Reproduced with permission [127]. Copyright 2020, American Chemical Society. (b) POM grafting on graphene through metal-O bond. Reproduced with permission [128]. Copyright 2022, Elsevier. (c) Covalent modification of CNTs with SiW_{11}-NH_2. Reproduced with permission [129]. Copyright 2014, Royal Society of Chemistry. (d) SiW_{11} grafted with pyrene by Si-N bond is connected to CNT through π-π stacking interaction. Reproduced with permission [48]. Copyright 2013, Wiley-VCH. (e-h) HRTEM images of $MnMo_6$–$2NH_2$–GO-2 [127], rGO/POM [128], CNTs-SiW_{11} [129] and SWNTs/Py–SiW_{11} [48]. The pink circle represents the agglomeration of POM particles.

~1.1 nm, in which both the covalently linked $MnMo_6$–$2NH_2$ electron sponge and the covalent bond electron bridge are highly adventurous for battery applications. It shows excellent rate capability (301 mAh/g in 5 A/g) and good stability (the capacity retention is nearly 100% at 1000 mA/g over 500 cycles) for LIBs. In addition to using metal nitrogen as a bridge, Hwang *et al.* also connected POM molecules with graphene sheets through metal-oxygen bonds (Fig. 7b), which gives full play to the synergistic effects of graphene and POM. An all-redox active hybrid SCs cell with rGO-POM cathode and MXene anode exhibit a maximum specific energy and power of 50.46 Wh/kg and 7000 W/kg [128]. However, direct covalent linking POM onto graphene not only destroys the structure of POMs to a certain extent, but also opens the sp^2 hybrid orbital of graphene, resulting in blocked electron transport between POMs and the substrate.

POMs-CNT by covalent linking: Recently, linking CNT and SiW_{11} also has been realized by covalent amide bonds created through the reaction of acyl chloride-functionalized CNTs with POMs functionalized by organo-amine (Fig. 7c) [129]. The CNTs/NH_2–SiW_{11} nanocomposite exhibits high capacity, good capacity retention and cycling stability as anode material in LIBs. Besides, Song *et al.* also covalently coupled Keggin POMs with the ligand pyrene through a metal-nitrogen bond, which was then coupled with SWCNTs through a strong π-π stacking interaction (Fig. 7d). The SWNTs/Py-SiW_{11} also manifests higher discharge capacity, and better rate capacity and cycling stability than the individual components as anode material in LIBs [48]. Although the electrochemical performance of the composites was enhanced by such stable binding, there is still the problem of low covalent grafting rate [130]. It should be noted that all these POMs clusters were observed by transmission electron microscope (TEM) as shown in Figs. 7e-h, exhibiting the occurrence of aggregation. In fact, it is difficult to determine the single Keggin-POM molecule with size smaller than 1.0 nm by TEM because of its resolution and sensitivity limitations [131]. Covalent ligation may also destroy the structure of POMs themselves, which is not conducive to the excitation of intrinsic activity and the improvement of electrochemical performance. Although nonconfinement strategies have been achieved some progress in immobilizing POMs on conductive supports, the agglomeration problems, and the lack of studies on intrinsic activity of real single POM molecule hinders the further development of POMs. Additionally, direct observations of POMs molecule configurations can help to better understand interactions and to analysis mechanism at the atomic scale [132].

Based on the above analysis, connecting POMs with supports by covalent or non-covalent linking has achieves certain success for improving the performance of POMs for electrochemical energy storage. The electrochemical performance of supported POMs is given in Tables 1 and 2 [133]. For a single POM cluster, if each reaction site of a single molecule can be guaranteed to be homogeneous, then the corresponding energy storage or catalytic system should possess a thermodynamic optimum at a single molecule or even a single atom level. That is, if the design of individual molecular clusters is sufficiently elaborate, the recognition and interaction of molecules can be more specific. Therefore, precise confinement of POMs is needed to explore more new phenomena, new systems, new mechanisms, and new applications. Compared with the synergy between multiple components, a single POM molecule by confinement would stimulate more application potential.

The rate of material transport, especially the rate of diffusion and migration, is highly dependent on the local microenvironment. Compared with non-confinement strategy, the nanopore-encaged POMs exhibit superior electrochemical performance as well as high stability endowed due to the stimulation of intrinsic activity by the host [50]. In addition, the synergistic effect of confined POMs and host frameworks can further promote the electrochemical performance of confined system. POMs confined in organic and inorganic substrates have played increasing important roles in the field of energy storage. So, considering the great advantages of both POMs and conductive substrates, the fabrication of confined structures is more attractive, and the excellent performance is also expected from these systems with more accessible active sites.

3.2. Confinement

In recent years, organic porous materials with uniform porous structures (*e.g.*, organic polymer hydrogel [134], MOFs [135] and COFs [11,136]) as well as inorganic porous martials (*e.g.*, CNTs [137] and PC [50]), have been used to confine and stabilize POMs to investigate more fundamental mechanisms. This section provides an overview on the different nanomaterials on dispersibility, structure, electronic properties, and electrochemical energy storage performance of confined POMs. It should be noted that even weak van der Waals interactions in confined space can strongly influence the behaviors of single POM molecule [138,139].

3.2.1. Confinement in organic substrates

As we known, organic nano porous materials (*e.g.*, MOFs, MOFs) have been proven to be ideal substrates to confine POMs [140,141], because MOFs possess orderly distributed small pores (<3 nm) [142] and good stability [143,144]. While it should be noted that confinement of POM cluster is generally achieved by screening subject porous materials with appropriate pore sizes.

POMs confined in MOFs/COFs: The dissolution of POMs can also be prevented by embedding them in the MOF cavity, because they have fully complementary dimensions [145–147]. For example. the diameter of the ZIF-67 cavity is about 1.16 nm while size of the Keggin-POMs is about 1.0 nm [148]. Since first utilization of POMOF in rechargeable LIBs for the first time, there appeared numerous MOF-based POM applications in energy storage [149]. Sharma *et al.* prepared POM@ZIF-67 composites by one-step in situ synthesis strategy, which shows excellent supercapacitor

Table 1
Electrochemical performance of supported POMs-based SCs.

Supported POMs	Capacitance (Three-electrode)	Energy densities (Device)	Power densities (Device)	Cycle life	Ref.
PW_{12}@PPy	434 mF/cm^2	2.33 mWh/cm^3	54 mW/cm^3	Capacity retention of 83%–84% over 5000 cycles with charge/discharge cycles at 11 mA/cm^2	[74]
PMo_{12}@PPy	374 mF/cm^2	1.5 mWh/cm^3	47 mW/cm^3		
PMo_{12}/PPy	400 F/g	–	–	–	[79]
AC–PW_{12}	254 F/g	4.96 Wh/kg	115 kW/kg (Max.)	98% capacitance retention after 30000 cycles at 6 A/g	[86]
PMo_{12}/AC	285 F/g	10.2 Wh/kg	15.5 kW/kg	–	[88]
PPy-PMo_{12}/rGO	360 F/g	–	–	–	[95]
PPD-PMo_{12}@rGO	790 F/g (1 mV/s)	–	–	Capacity retention of 90.5% after 30000 cycles	[96]
PMo_{12}/PIL/RGO	456 F/g (10 mV/s)	56 Wh/kg	52 kW/kg	98% retention of the capacitance with GCD cycles at 10 A/g	[97]
Mo_{132}-DTAB-EEG	65 F/g (1 mV/s)	–	–	Capacity retention of ~99% (5000 cycles at 100 mV/s)	[98]
SWCNT-TBA-PV_2Mo_{10}	224 mF/cm^2 (1 mA/cm^2)	15.4 Wh/kg	15.7 kW/kg	Retaining 95% of its specific capacitance after 6500 cycles	[26]
MWCNT/PMo_{12}/$SiMo_{12}$	2.68 ± 0.34 F/cm^2 (50 mV/s)	–	–	–	[105]
MWCNT/$SiMo_{12}$/PMo_{12}	1.93 ± 0.20 F/cm^2 (50 mV/s)				
GeMoV-PDDA-CpLum-CNT	80.7 ± 6.5 F/cm^3 (100 mV/s)	–	–	–	[106]
$PMo_{10}V_2$-MWCNT	88 F/cm^3	–	–	–	[108]
PMo_{12}–MWCNT	84 F/cm^3				
Dual-layer MWCNT	158 F/cm^3 (100 mV/s)				
MWCNT-PIL-$GeMo_{12}$	85 F/cm^3	–	–	PIL dual layer composite maintained over 70% of this capacitance at a fast rate of 2 V/s	[109]
MWCNT-PDDA-$GeMo_{12}$	111 F/cm^3				
MWCNT-PIL/$GeMo_{12}$–$SiMo_{12}$	191.2 F/cm^3 (100 mV/s)				
MXene/AC/TEAPW_{12}	87 F/g (1 mV/s)	14.2 Wh/kg	540 W/kg	92% of its initial capacitance remained after 10,000 cycles at 1 A/g	[118]
$[Zn(itmb)_3H_2O]_2^{4+}$/SiW_{12}@$Ti_3C_2T_x$	1480 F/g (5 A/g)	32.2 Wh/kg	2397.5 W/kg	Capacity retention of 79.0% after 10000 cycles at 20 A/g	[119]
VM POMs/MXenes		195.5 Wh/kg	380 W/kg	Capacity retention of 80.0% after 1200 cycles at 0.6 A/g	[120]
POMs-PPy	53 F/g (250 mV/s)			Retain 95% of its initial capacitance over 1200 cycles	[125]
rGO-PMo_{12}	631 F/g (5 A/g)	50.46 Wh/kg	7000 W/kg	Capacitance retention of 87.12% over 10,000 cycles	[128]

Table 2
Electrochemical performance of supported POMs-based batteries.

Battery	Composite material	Voltage window (V)	Specific capacities [a]	Cycle life	Ref.
Li-ion batteries	PVIMo–ZnPOM/C/S	1.6—3.0	1450 mAh/g (0.5 C)	Capacity retention of 97.6% after 120 cycles	[75]
	POM/RGO(PMo_{12}/RGO)	1.5—4.2	140 Ah/kg	–	[92]
	$[Co_4W_{18}]$/rGO/S	2.7—1.8	1251 mAh/g (0.168 A/g$_s$)	Capacity fading of 0.015% per cycle after 1000 cycles at 2 C (*i.e.*, 3.36 A/g)	[99]
	POM/SWNT($TBA_3[PMo_{12}O_{40}]$)	1.5—4.2	320 Ah/kg	–	[103]
	$MnMo_6$–$2NH_2$–GO-2	0—3.0	1642 mAh/g (100 mA/g)	Capacity retention is nearly 100% at 1000 mA/g over 500 cycles	[127]
	CNTs–SiW_{11}	0—3.0	650 mAh/g (0.5 mA/cm^2)	Capacitance remains stable up to 100 cycles	[129]
	SWNTs/Py–SiW_{11}	0—3.0	580 mAh/g (0.5 mA/cm^2)	Discharge capacity of 580 mAh/g ramains for up to 100 cycles	[48]
	SWNT/Anderson nanocomposite	0—3.0	1287.8 mAh/g (0.5 mA/cm^2)	Capacity retention of 27.4% for 100 cycles	[130]
	Co-PMo/CNTs	0—3.0	820 mAh/g (0.5 mA/cm^2)	Capacity barely loss after the initial decay for 450 cycles at 2000 mA/g	[133]
Na-ion batteries	MF POMs/MXenes//AC	–	58.7 Wh/kg	~99% capacity retention after 800 cycles at 1.0 A/g	[115]

[a] Specific capacities of battery are all recorded after the initial capacity loss.

performance. This complementary dimensional cavity and sharing of ammonium decavanadate resulted in tighter binding of POMs and ZIF-67 [141]. However, MOF has low electrical conductivity and is not conducive to electrochemical applications. In a recent work, POMs are immobilized in MOF cages by one-step hydrothermal synthesis strategies to avoid the leaching of POMs (Figs. 8a and b). To enhance the conductivity, ILs was introduced into the POMs@MOF by anion-exchange reaction. As shown in Fig. 8c, the $PMo_{10}V_2$-ILs@MIL-100 as the anode material for LIBs, shows superior high-rate capability and cycling stability (maintains a capacity of about 600 mAh/g after 400 cycles at 1 A/g) [150]. Also, POMs were confined into three-dimensional metal organic carbene frameworks (MCNCs) by hydrothermally route. Similarly, in order to improve the electrical conductivity, they were combined with the SWNTs and the reversible multielectron redox behavior and electron storage functions of POMs are guaranteed (Figs. 8d and

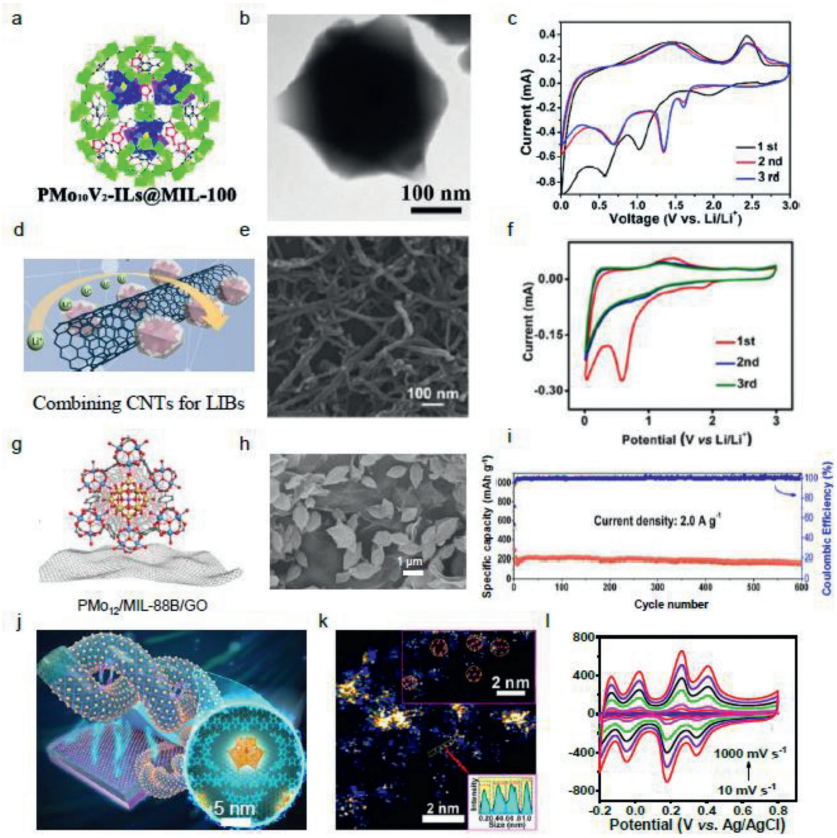

Fig. 8. Confinement of POM in organic nano-porous materials. (a-c) Molecular model and TEM image of $PMo_{10}V_2$-Ils@MIL-100 crystals. Corresponding CV profiles at a scan rate of 0.1 mV/s. Reproduced with permission [150]. Copyright 2018, Royal Society of Chemistry. (d-f) Molecular model and SEM image of POMs@MCNCs/SWNT composites. Corresponding CV profiles in the range of 0.01–3 V at a scan rate of 0.1 mV/s. Reproduced with permission [151]. Copyright 2018, American Chemical Society. (g-i) Van der Waals loading PMo_{12}/MIL-88B onto GO and corresponding STEM image, as well as cycling stability of PMo_{12}/MIL-88B-based Li-S batteries. Reproduced with permission [99]. Copyright 2022, Nature Publishing Group. (j-l) One-step *in situ* confine PMo_{12} in PPy/CNT hydrogel and STEM images of PMo_{12}/PPy/CNT hydrogel, as well as CV curves of PMo_{12}/PPy/CNT at different scan rates [33]. Reproduced with permission [33]. Copyright 2020, Royal Society of Chemistry.

e). The obtained POMs@MCNCs/SWNT composite excellent electrochemical performance and good stability as anode materials of LIBs (Fig. 8f) [151]. In a recent study, surfactant-assisted media is also used to confine POMs in MOFs. Also, by a simple sonication-driven functionalization strategy, to overcome the poor conductivity of POMs@MOF, the POMs@MOF was also loaded on the CNT, achieving increased effective sites and excellent conductivity [133]. Besides, recently, PMo_{12} clusters confined by MOF (MIL-BB) was also supported onto conductive substrate of RGO by continuous sonication based on van der Waals forces (Figs. 8g and h). Due to their reversible multielectron redox property and high ionic conductivity, the PMo_{12}/MIL-88B/GO composites show a high coulombic efficiency (51.0%) and an excellent capacity performance (214.2 mAh/g for 600 cycles at 2.0 A/g) for NIBs (Fig. 8i) [152]. Similarly, POM-based MOFs (POMOFs) supported on RGO was also prepared for LIBs by Professor Lan's group. Thanks to the multi-electron redox properties of POMs, open frameworks of MOFs, and high electronic conductivity of RGO, the resultant composite can buffer the volume expansion, leading to superhigh capacity and rate performances. Moreover, the hybrid also demonstrates the hybrid behavior of battery and supercapacitor [149]. However, as shown in Figs. 8b, e and h, because MOF is not resistant to radiation, it is difficult to observe the dispersed particles in the electron microscope image as given in the report [140,153–155].

POMs confined in conductive polymer hydrogel: Compared to traditional polymer, hydrogels are usually synthesized with crosslinker as "bridges" between polymer chains. Different from traditional conductive polymers, conductive polymer hydrogels (CPH) possess more excellent properties [156,157]. Specifically, CPH possess the characteristics of both conductive polymers and unique advantages endowed by their structure [158]: (1) 3D structure providing a conductive and mechanically robust framework; (2) Continuous conductive backbones promoting charge transport; (3) Porous structure accelerating the diffusion of ions and molecules; (4) Expansion property delving an additional effective interface between the molecular chain and the solution phase. In addition to physical and morphological properties, conductive polymer hydrogels also manifest improved mechanical properties [159], which can even be controlled by changing crosslinker molecules to achieve supramolecular self-assembly [156]. These excellent properties make conductive polymer hydrogel an ideal substrate for supporting or confining POMs. Accordingly, in recent studies, our group achieved a supramolecular confinement of single PMo_{12} clusters in a PPy hydrogel-wrapped CNT framework by space-electrostatic confinement interactions (Fig. 8j) [33], Specifically, we first calculated the interaction between the cross-linking agent tetrafunctional group (4-carboxyphenyl)porphyrin (TCPP) and PPy through density functional theory [160], and found that the space distance of the pore connected by TCPP and PPy is about 1.8 nm, which can obviously confine Keggin-type POM molecules (~1.05 nm). The color enhanced Z-contrast SEM image results show uniform distribution of PMo_{12} (Fig. 8k), exhibiting excellent rate performance of SCs (Fig. 8l) and better cycling performance than the traditional composite materials in the charge-discharge process. Clearly, this strategy can be expanded to confine various POMs with size of ~1 nm. In fact, due to the general conductivity

of the polymer, a lot of effort is also spent in the process of collecting electron microscopy pictures of PMo_{12} in this hybrid hydrogel. Reductions of the accelerating voltage and the exposure time as well as careful control of the electron beam current can be applied to obtain high-resolution imaging of POMs in the hybrid hydrogel [155,161].

3.2.2. Confinement in inorganic substrates

As mentioned above, due to the limitation of detection technology, the chemical structures of the POMs-substrate interface have not been completely understood [162,163]. Therefore, most experimental studies focus on the macroscopic properties of composites, and the mechanism is still need to be studied [164]. Recently, both operando X-ray absorption fine spectra [63] and solid-state nuclear magnetic resonance (NMR) spectroscopy [165,166] have been performed to understand the interact mechanisms between POMs and substrates. It is impressive to electrically "connect" individual POM molecules to the conductive substrates to maximize its electron transfer activities. Moreover, the inorganic conductive substrate is more resistant to radiation, and it is more conducive to the collection of electron microscopy samples of POMs clusters on conductive substrates (*e.g.*, CNT). In recent years, exploring more conductive substrate with precise cage or pore to confine single POM molecule to address the global energy challenges is also in processing.

POMs confined in CNT: In addition to the organic nano porous supports, recently, connecting POMs with an arc-discharge SWNTs with average diameters of 1.4 nm also has been reported [167,168]. In order to fill the CNT with POMs, a high concentration of acid was used to open the seal of the CNT [137]. Then the CNT encapsulated POMs was obtained by ultrasound it with POMs solution. Studies have shown that spontaneous redox reaction between POMs and CNT is a driving force for encapsulating [169]. It should be noted that the encapsulation of POMs of negative charge into the SWNTs with positive charge is mainly attributed to the transferred electron from the host to the inner guests (Fig. 9a). Besides, POM in one dimensional CNT can make better use of the proton conductivity of CNT, which shows relative-stable electrochemical performance (Fig. 9b). As shown in Fig. 9c, the dark-contrast POMs are 1.0–1.8 nm wide, indicating different orientations of POMs within the SWNT cavities [23]. However, encapsulated POM is completely covered by CNT, not only obstructing their interaction with the environment, but also reconfigures the electron of POMs [170]. Clearly, it is not conducive to the perfect exposure of POM active sites in electrochemical applications, limiting the improvement of electrochemical performance. Therefore, encapsulated POMs in CNT are mostly used in the screening of CNT and other applications [137]. Despite significant progress being made in the synthesis technologies of CNTs with different diameters and morphologies, the confinement of POMs is still be limited by the size of the CNT.

POMs confined in micro-PC: In fact, local structural image information of single POM cluster within crystalline conductive nano porous materials can be detected by Cs-corrected high angle dark field spherical aberration electron microscope. However, the temporary or permanent destroy of MOF or polymer hydrogel can be caused by the highly energetic electron beam, which limits the determining of confined POMs in the framework [140,171]. Accordingly, carbon materials, especially PC, become ideal confined substrates owing to their high conductivity and excellent stability [172]. Considering the developments, in early 2022, we precisely confined Keggin-type POM molecules in a designed micro-PC with unique super-micropore of ~1.09 nm (Fig. 9d) [50]. As shown in Fig. 9c, homogeneously distributed bright dots of uniformly distributed PMo_{12} with size of ~0.70 ± 0.05 nm are observed in PMo_{12}@micro-PC. Due to the precise confinement, the

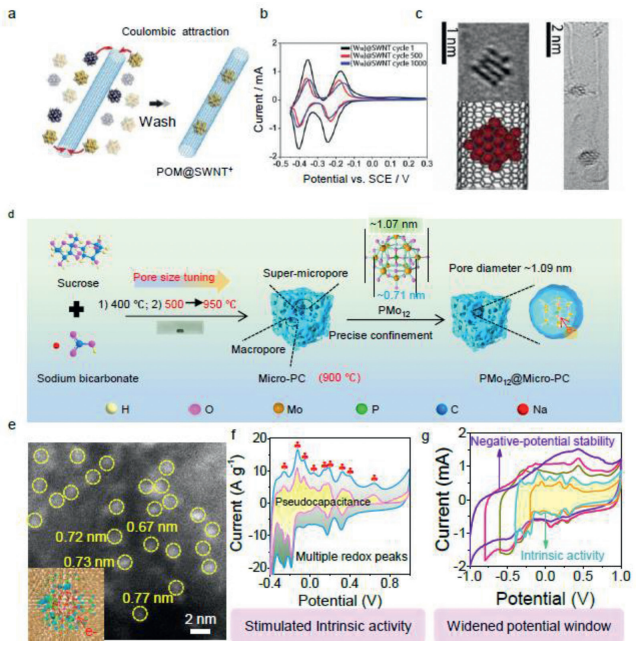

Fig. 9. (a) Encapsulating POMs in SWNTs by spontaneous redox reaction. (b) Electrochemical performance of POM@SWCNT. (c) Corresponding TEM images, and molecular models of POMs@SWCNTs. Reproduced with permission [169]. Copyright 2022, John Wiley and Sons Ltd. (c) Schematic view of the precise confinement of PMo_{12} in micro-PC. (d) Schematic illustration of the precise confinement of PMo_{12} in micro-PC. (e) High-angle annular dark-field scanning TEM image of PMo_{12}@micro-PC. (f, g) CV curves of PMo_{12}@micro-PC at different potential ranges. Reproduced with permission [22]. Copyright 2022, Wiley-VCH. All copied with permission.

confined POM molecule delvers an unpresented multi-electron redox-activity. By DFT causation, it was found that the sufficient activity center exposure and maximum electron-transfer from PC host to POMs guest stabilizes the confined guest molecule (Fig. 9c inset). This precise confinement optimizes the active electronic states of POMs (Fig. 9e) and broadens the potential window (Figs. 9f and g). Compared to traditional POM-carbon materials, the precise confinement of POM in PC leads to a higher capacitance. This micro-PC shows prominent advantages in confining and stabilizing Keggin-type POMs, which suggest a future research's directions for confined POMs in energy fields. The specific values for the energy/power densities and cycle life of confined-POMs have been summarized in Tables 3 and 4. Clearly, when the POM behaviors in single-molecule state, the scale in nanoscale, what we see in the electron microscopy may not be a true local structure. If the detection accuracy is not improved and only the overall average performance of the material is pursued, the statistical distribution of single molecules or even single atoms cannot be reflected. Therefore, there are higher requirements for characterization from manometers to angstroms, spatial resolution, and detection data acquisition rate. *In situ* characterization techniques such as pump-probe X-ray detection can provide a glimpse into the process of electron transfer, which can be used to study the electron transfer interaction between POMs and substrates.

4. Summary and outlook

This review briefly summarizes the recent progress from surface loading to precise confinement of POMs for mainstream electrochemical energy storage applications. The advantages and disadvantages of different loading strategies have been summarized in Table 5. According to the loading strategy, surface loading and precise confinement strategies are applied to taking advantage of

Table 3
Electrochemical performance of confined POMs-based SCs.

Confined POMs	Capacitance (Three electrode)	Energy densities	Power densities	Cycle life	Ref.
POMs@ZIF-67	–	19.7 Wh/kg	1342.6 W/kg	89% for 5000 cycles	[141]
$PMo_{10}V_2$@ZIF-67	765 F/g (5 mV/s)	20.9 Wh/kg	702 W/kg	Cycling retention of 106.4% after 5000 cycles at 5 A/g	[148]
PMo_{12}/PPy/CNT	1170 F/g (1 A/g)	67.5 μWh/cm^2	700 μW/cm^2	Capacitance retention of 85.7% after 3000 cycles	[33]
PMo_{12}/PPy	776 F/g (0.5 A/g)	50.66 Wh/kg	750 W/kg	80% for 1000 cycles	[160]

Table 4
Electrochemical performance of confined POMs-based batteries.

Battery	POM composite material	Voltage window (V)	Specific capacities (mAh/g)	Cycle life	Ref.
Li-ion batteries	$PMo_{10}V_2$/RGO	0.01—3.0	1519 (50 mA/g)	~70% capacity remains after 100 cycles	[149]
	$PMo_{10}V_2$-ILs@MIL-100	0.01—3.0	1114 (0.1 A/g)	The capacitance has hardly dropped after 100 cycles at 0.1 A/g	[150]
	PW_{12}@MCNCs-1/SWNT	0—3.0	859 (0.1 A/g)	Even after 70 cycles, the reversible capacity remains at ~93%	[151]
	PMo_{12}/MIL-88B/GO	0.01—3.0	859 (0.1 A/g)	214.2 mAh/g for 600 cycles at 2.0 A/g	[152]
Na-ion batteries	PMo_{12}/MOFs/GO	0.01—3.0	430 (0.2 A/g)	Stabilized at 288.2 mAh/g after 100 cycles	[153]
	PMo_{12}@SWNT	0—3.0	210 (0.75 A/g)	~100%	[170]

Table 5
Strengths and weaknesses of non-confinement and confinement strategies.

Strategies for supported POMs		Advantages		Disadvantages
Non-confinement	Non-covalent interaction	Overcoming solubility issues	Simple preparation	Weak interaction between POMs and substrate which cause the reunion and shedding of POMs
	Covalent interaction		Stronger interaction Stable on substates	Destroying the structure of POMs Reducing the overall conductivity
Confinement	Organic substrates	Overcoming solubility issues Stimulating intrinsic activity	Adjustable matching size Abundant variety	Imaging of the structure under typical conditions is difficult The substrate is not radiation resistant
	Inorganic substrates		More stable structure Stronger conductivity	Micro size is difficult to control Intrinsic activity mechanism is difficult to analyze

the "semipermeable molecular capacitor" redox behaviors and the high stability of the redox states of POMs in energy storage applications. In the past decades, various POMs-based composites have been designed as high-performance electrode materials in energy storage fields. The interactions between POMs and substrates include non-covalent interaction and covalent interaction. According to the geometric relationships between POMs and supports, it can be divided into confinement and non-confinement. Through this review, we show how the geometric relationships and interactions between materials affect the final properties and states of POMs. Compared with loading by covalent or non-covalent interaction, the precise confinement of POMs renders them stimulated activity and more exposed active sites. However, there are fewer conductive substrates available for the precise confinement of POMs, so further rational designing of suitable cage for confinement of POMs is needed. In addition, despite the significant progress that has been made, it remains big challenges of the confined POMs for electrochemical-rated fields. Exploiting novel properties caused by precise confinement of POMs is needed. It is a very important and attractive issue to realize the single-molecule dispersion of POMs on the conductive supports for fully stimulating their intrinsic activity.

(1) Exploiting novel properties caused by precise confinement of POMs is needed. In the non-confined strategy, the agglomeration and shedding of POMs are extremely difficult to avoid due to the mismatch of pore with the molecule size of POMs. It is a very important and attractive issue to exploit the synergistic effects between POMs and support to improve their electrochemical performance. Notably, further exploiting novel properties of conductive supports caused by precise confinement of POMs, to deeply study the electronic transmission interaction between them is highly challenging. Furthermore, the electronic transmission interaction from host to guest endowed by precise confinement may also bring new electrochemical inherent properties even for traditional electrochemical reaction. Besides, the combination of space-coordination interactions or space electron interactions is expected to confine POMs stably, which can inspire us to explore more intrinsic activities of POMs for advanced electrochemical energy storage systems.

(2) Advanced characterization technologies (*i.e.*, pump probe X-ray detection) as well as computational simulations are required in the future. For more atomic scale evidence of confined single POM molecule and intrinsic properties, as well as interface electron transfer between POMs and supports, more advanced characterization technologies is request. Because one of the advantages of POMs is that single-molecule clusters facilitate the study of their structure-activity relationships. Secondly, the precise confinement of multiple POM molecules into the novel designed conductive substrate is expected to stimulate the interaction of different POM molecules in the same one confined system. Because this multiple-confinement of POMs would endow the electronic structure and geometric structure of the outer orbital of single metal atom (*e.g.*, Mo from PMo_{12}) with tunable and richer structural parameters. However, the characterization tools for multi-cluster are far from insufficient, and the synthesis strategies are also insufficient, and it is difficult to achieve ultra-high dispersion and regulation of every single molecule active site.

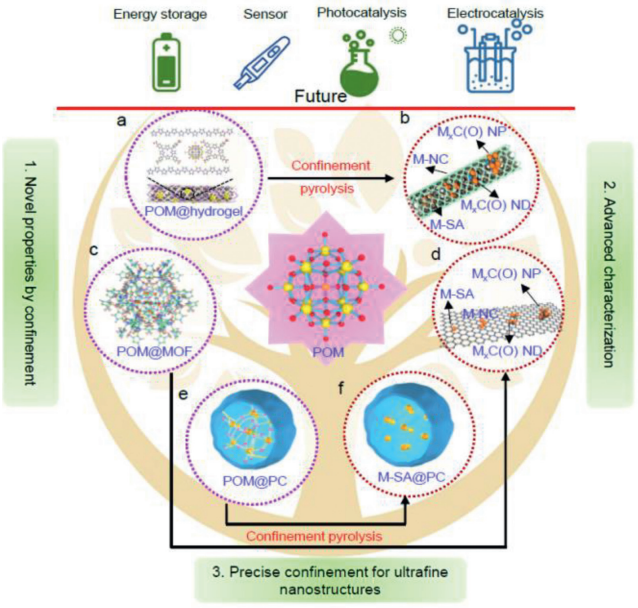

Fig. 10. Outlook for confined POMs. Pyrolysis of confined POMs to construct ultrafine nanostructures for efficient photo/electrochemical applications.

(3) The precise control of spatial separation of individual metal nanostructure with different sizes is promising. We believe that MOF/COF or polymer hydrogel cage confined-POMs can serve as perfect precursors to construct various ultrafine nanostructures. The ultrafine metal-based nanostructures with different scales can be obtained by pyrolysis confined POMs with different confinement amounts (Figs. 10a-d) [173]. This would expand its application in the future. Specially, the precise confinement of POM in micro-PC would be a perfect precursor to construct non-noble single atom confined in PC (bottom in Figs. 10e and f). Furthermore, more novel, and facile artificial cages or pores for confining POMs are extremely desirable to precisely control the size of ultrafine non-precious metal nanostructures. In addition, as we known, the 4-fold hollow site on the POM cluster is a stable binding site for the metal single atom [174]. However, agglomeration of POM is unfavorable for this binding. So, the metal sites are need to be stabilized by POMs. We believe the confined POMs (Figs. 10a, c and e) would be a novel substrate to achieve more fast electron transfer kinetics in electrocatalysis fields by further anchoring metal atoms. We also believe that the abundant tunable properties of confined single POM molecule may give us hope to solve the problems of high energy consumption and high pollution in traditional catalysis or energy storage processes. In the context of dual-carbon, this requires the joint efforts of everyone to promote the progress and healthy development.

Declaration of competing interest

The authors declare that they have no known competing financial interests or personal relationships that could have appeared to influence the work reported in this paper.

Acknowledgments

C. Wang and Y. Song contributed equally to this work. The authors acknowledge the National Natural Science Foundation of China (Nos. 51902222 and 62174013), The Central Government Guides Local Funds for Science and Technology Development (No. YDZJSX2022A021), National Natural Science Foundation of China (No. 52201019), Scientific and Technological Innovation Programs of Higher Education Institutions in Shanxi (STIP, No. 2022L036).

References

[1] A.D. Easley, T. Ma, J.L. Lutkenhaus, Joule 6 (2022) 1743–1749.
[2] S. Tang, M. Ma, X. Zhang, et al., Adv. Funct. Mater. 32 (2022) 2205417.
[3] W. Sun, Z. Xu, C. Qiao, et al., Adv. Sci. 9 (2022) e2201679.
[4] Z.W. Seh, J. Kibsgaard, C.F. Dickens, et al., Science 355 (2017) eaad4998.
[5] D.D. Zhang, Z.Y. Guo, P.F. Guo, et al., ACS Appl. Mater. Interfaces 10 (2018) 21876–21882.
[6] B. Dunn, H. Kamath, J.M. Tarascon, Science 334 (2011) 928–935.
[7] Q. Chen, L. Tan, S. Wang, et al., Electrochim. Acta 385 (2021) 138385.
[8] C. Fang, J. Li, M. Zhang, et al., Nature 572 (2019) 511–515.
[9] R. Liu, C. Streb, Adv. Energy Mater. 11 (2021) 2101120.
[10] M.R. Horn, A. Singh, S. Alomari, et al., Energ. Environ. Sci. 14 (2021) 1652–1700.
[11] H. Liu, L.G. Gong, C.X. Wang, et al., J. Mater. Chem. A 9 (2021) 13161–13169.
[12] M. Lu, M. Zhang, J. Liu, et al., J. Am. Chem. Soc. 144 (2022) 1861–1871.
[13] A. Bayaguud, K. Chen, Y. Wei, Nano Res. 9 (2016) 3858–3867.
[14] S. Kan, K. Nakajima, T. Asai, M.A. K.asaya, Adv. Sci. 9 (2022) 2104076.
[15] M. Kourasi, R.G.A. Wills, A.A. Shah, F.C. Walsh, Electrochim. Acta 127 (2014) 454–466.
[16] Y. Watanabe, K. Hyeon Deuk, T. Yamamoto, et al., Sci. Adv. 8 (2022) eabm5379.
[17] N.I. Gumerova, A. Rompel, Nat. Rev. Chem. 2 (2018) 0112.
[18] H.N. Miras, L.V. Nadal, L. Cronin, Chem. Soc. Rev. 43 (2014) 5679–5699.
[19] V.M.T. Pope, Angew. Chem. Int. Ed. 96 (1984) 730 –730.
[20] Y. Geng, K. Jin, J. Mei, et al., J. Hazard. Mater. 382 (2020) 121032.
[21] H. Gao, H. Wu, K. Lian, Electrochem. Commun. 17 (2012) 48–51.
[22] Y. Nishimoto, D. Yokogawa, H. Yoshikawa, K. Awaga, S. Irle, J. Am. Chem. Soc. 136 (2014) 9042–9052.
[23] J.W. Jordan, G.A. Lowe, R.L. McSweeney, et al., Adv. Mater. 31 (2019) e1904182.
[24] Y. Liu, X. Wu, Z. Li, et al., Nat. Commun. 12 (2021) 4205.
[25] S. Chen, Y. Xiang, M.K. Banks, et al., Nanoscale 10 (2018) 20043–20052.
[26] H.Y. Chen, R. Al Oweini, J. Friedl, et al., Nanoscale 7 (2015) 7934–7941.
[27] R. Liu, G. Zhang, H. Cao, et al., Energ. Environ. Sci. 9 (2016) 1012–1023.
[28] S. Herrmann, C. Ritchie, C. Streb, Dalton Trans. 44 (2015) 7092–7104.
[29] M.H. Yang, B.G. Choi, S.C. Jung, Y.Y. Han, B.L. Sang, Adv. Funct. Mater. 24 (2015) 7301–7309.
[30] Y.Y. Chen, M. Han, Y.J. Tang, et al., Chem. Commun. 51 (2015) 12377–12380.
[31] M. Genovese, K. Lian, J. Mater. Chem. A 5 (2017) 3939–3947.
[32] V. Prabhakaran, B.L. Mehdi, J.J. Ditto, et al., Nat. Commun. 7 (2016) 11399.
[33] M. Wang, Y. Zhang, T. Zhang, et al., Nanoscale 12 (2020) 11887–11898.
[34] A. Botos, J. Biskupek, T.W. Chamberlain, et al., J. Am. Chem. Soc. 138 (2016) 8175–8183.
[35] R.Y. Li, J.J. Zhang, Z.P. Wang, et al., Sensor. Actuator. B: Chem. 208 (2015) 421–428.
[36] G.P. Maria, G.M. Catherine, R.M. Benedikt, L.K.P. Mialane, J. Am. Chem. Soc. 140 (2018) 3613–3618.
[37] H. Liu, L. Chang, C. Bai, Angew. Chem. Int. Ed. 55 (2016) 5019–5023.
[38] V. Ortalan, A. Uzun, B.C. Gates, N.D. Browning, Nat. Nanotechnol. 5 (2010) 506–510.
[39] X. Xu, S. Chen, Y. Chen, et al., Small 12 (2016) 2982–2990.
[40] S. Yang, M. Wang, Y. Zhang, et al., Energy Environ. Mater. 6 (2023) e12396.
[41] G. Bidan, E.M. Genies, M. Lapkowski, J. Electroanal. Chem. 251 (1988) 297–306.
[42] P. Judeinstein, Chem. Mater. 4 (1992) 4–7.
[43] B. Sulikowski, J. Haber, A. Kubacka, et al., Catal. Lett. 39 (1996) 27–31.
[44] N.I. Kovtyukhova, P.J. Ollivier, B.R. Martin, et al., Chem. Mater. 11 (1999) 771–778.
[45] G. Ferey, C.M. D.raznieks, C. Serre, et al., Science 309 (2005) 2040–2042.
[46] D. Pan, J. Chen, W. Tao, L. Nie, S. Yao, Langmuir 22 (2006) 5872–5876.
[47] J. Sloan, G. Matthewman, C.D. Smith, et al., ACS Nano 2 (2008) 966–976.
[48] D. Ma, L. Liang, W. Chen, H. Liu, Y.F. Song, Adv. Funct. Mater. 23 (2013) 6100–6105.
[49] H. Ma, B. Liu, B. Li, et al., J. Am. Chem. Soc. 138 (2016) 5897–5903.
[50] Y.F. Liu, C.W. Hu, G.P. Yang, Chin. Chem. Lett. 34 (2023) 108097.
[51] C. Boskovic, Acc. Chem. Res. 50 (2017) 2205–2214.
[52] J. Gautam, Y. Liu, J. Gu, et al., Adv. Funct. Mater. 31 (2021) 2106147.
[53] J.A. Monge, B.E. Bakkali, G. Trautwein, S. Reinoso, Appl. Catal. B: Environ. 224 (2018) 194–203.
[54] Q. Liu, P. He, H. Yu, et al., Sci. Adv. 5 (2019) eaax1081.
[55] L. Yang, J. Lei, J.M. Fan, et al., Adv. Mater. 33 (2021) e2005019.
[56] N.V. Izarova, M.T. Pope, U. Kortz, Angew. Chem. Int. Ed. 51 (2012) 9492–9510.
[57] L. Chen, X.J. Sang, J.S. Li, et al., Inorg. Chem. Commun. 47 (2014) 138–143.
[58] N. Mizuno, M. Misono, Chem. Rev. 98 (1998) 199–218.
[59] K. Yonesato, S. Yamazoe, D. Yokogawa, K. Yamaguchi, K. Suzuki, Angew. Chem. Int. Ed. 60 (2021) 16994–16998.
[60] Y. Liu, S. Lu, H. Wang, et al., Adv. Energy Mater. 7 (2017) 1601224.
[61] H.S. Yang, Y.C. Bai, D.H. Ouyang, et al., J. Energy Chem. 58 (2021) 133–146.
[62] L. Ni, G. Yang, Y. Liu, et al., ACS Nano 15 (2021) 12222–12236.
[63] H. Wang, S. Hamanaka, Y. Nishimoto, et al., J. Am. Chem. Soc. 134 (2012) 4918–4924.
[64] Y. Zhou, J. Yang, H. Su, et al., J. Am. Chem. Soc. 136 (2014) 4954–4964.

[65] J. Li, R. Guttinger, R. More, et al., Chem. Soc. Rev. 46 (2017) 6124–6147.
[66] S.W. Li, R.M. Gao, W. Zhang, Y. Zhang, J. Zhao, Fuel 221 (2018) 1–11.
[67] Z. Tong, M. Xu, Q. Li, et al., Talanta 220 (2020) 121373.
[68] N.V. Maksimchuk, O.A. Kholdeeva, K.A. Kovalenko, V.P. Fedin, Isr. J. Chem. 51 (2011) 281–289.
[69] I. Ullah, A. Munir, A. Haider, N. Ullah, I. Hussain, Nanophotonics 10 (2021) 1595–1620.
[70] H. Shirakawa, E.J. L.ouis, A.G. M.acdiarmid, C.K. C.hiang, A.J. Heeger, Chem. Commun. (1977) 578–580.
[71] J. Lutkenhaus, Science 359 (2018) 1334–1335.
[72] B. Liu, W. Zhao, Z. Ding, et al., Adv. Mater. 28 (2016) 6457–6464.
[73] W. Qi, L. Wu, Polym. Int. 58 (2009) 1217–1225.
[74] D.P. Dubal, B. Ballesteros, A.A. Mohite, P.G. Romero, ChemSusChem 10 (2017) 731–737.
[75] V. Singh, A.K. Padhan, S.D. Adhikary, et al., J. Mater. Chem. A 7 (2019) 3018–3023.
[76] S. Herrmann, N. Aydemir, F. Nägele, et al., Adv. Funct. Mater. 27 (2017) 1700881.
[77] L. Zhai, H. Li, Molecules 24 (2019) 3425.
[78] D. Wang, J. Jiang, M.Y. C.ao, et al., Nano Res. 15 (2021) 3628–3637.
[79] A. Cao, Z. Chen, Y. Wang, et al., Synth. Met. 252 (2019) 135–141.
[80] L. Borchardt, Q.L. Z.hu, M.E. Casco, et al., Mater. Today 20 (2017) 592–610.
[81] V. Pavlenko, S. Khosravi H, S. Żółtowska, et al., Adv. Mater. Sci. Eng. 149 (2022) 100682.
[82] K.S.W. Sing, D.H. Everett, R.A.W. Haul, et al., Pure Appl. Chem. 57 (1985) 603–619.
[83] K.P. Lakshmi, K.J. Janas, M.M. Shaijumon, Carbon 131 (2018) 86–93.
[84] Z. Kang, Y. Liu, C.H. Tsang, et al., Chem. Commun. (2009) 413–415.
[85] Y. Izumi, K. Urabe, Chem. Lett. 5 (1981) 663–666.
[86] J.S. G.uevara, V. Ruiz, P.G. Romero, J. Mater. Chem. A 2 (2014) 1014–1021.
[87] J.A. M.onge, G. Trautwein, S.P. E.sclapez, J.A. Maciá-Agulló, Micropor. Mesopor. Mat. 115 (2008) 440–446.
[88] P. Palomino, J.S. G.uevara, M. Olivares-Marín, et al., Carbon 111 (2017) 74–82.
[89] K.S. Novoselov, A.K. Geim, S.V. Morozov, et al., Science 306 (2004) 666–669.
[90] M.J. Allen, V.C. Tung, R.B. Kaner, Chem. Rev. 110 (2010) 132–145.
[91] V.P. Pham, H.S. Jang, D. Whang, J.Y. Choi, Chem. Soc. Rev. 46 (2017) 6276–6300.
[92] K. Kume, N. Kawasaki, H. Wang, et al., J. Mater. Chem. A 2 (2014) 3801–3807.
[93] D. Zhou, B.H. Han, Adv. Funct. Mater. 20 (2010) 2717–2722.
[94] D. Martel, M. Gross, J. Solid State Electrochem. 11 (2006) 421–429.
[95] Y. Chen, M. Han, Y. Tang, et al., Chem. Commun. 51 (2015) 12377–12380.
[96] J. Gao, M. Tong, Z. Xing, et al., Chem. Commun. 56 (2020) 7305–7308.
[97] M. Yang, B.G. Choi, S.C. Jung, et al., Adv. Funct. Mater. 24 (2014) 7301–7309.
[98] D. Pakulski, A. Gorczyński, W. Czepa, et al., Energy Storage Mater 17 (2019) 186–193.
[99] J. Lei, X.X. Fan, T. Liu, et al., Nat. Commun. 13 (2022) 202.
[100] F. Peng, Y. Liu, R. Cui, et al., Chin. Sci. Bull. 57 (2011) 225–233.
[101] M.S. Ahmed, B. Choi, Y.B. Kim, Sci. Rep. 8 (2018) 2543.
[102] O.A. Oyetade, R.J. Kriek, Electrocatalysis 11 (2019) 35–45.
[103] N. Kawasaki, H. Wang, R. Nakanishi, et al., Angew. Chem. Int. Ed. 50 (2011) 3471–3474.
[104] A. Giusti, G. Charron, S. Mazerat, et al., Angew. Chem. Int. Ed. 48 (2009) 4949–4952.
[105] T. Akter, K. Hu, K. Lian, Electrochim. Acta 56 (2011) 4966–4971.
[106] J. N'Diaye, S. Siddiqui, K.L. Pak, K. Lian, J. Mater. Chem. A 8 (2020) 23463–23472.
[107] D.V. Jawale, F. Fossard, F. Miserque, et al., Carbon 188 (2022) 523–532.
[108] G. Bajwa, M. Genovese, K. Lian, ECS J. Solid State Soc. 2 (2013) M3046.
[109] M. Genovese, K. Lian, ACS Appl. Mater. Interfaces 8 (2016) 19100–19109.
[110] J. Hu, F. Jia, Y. Song, Chem. Eng. J. 326 (2017) 273–280.
[111] M. Naguib, M. Kurtoglu, V. Presser, et al., Adv. Mater. 23 (2011) 4248–4253.
[112] M.R. Lukatskaya, O. Mashtalir, C.E. Ren, et al., Science (2013) 1502–1505.
[113] J. Jiang, S. Bai, J. Zou, et al., Nano Res. 15 (2022) 6551–6567.
[114] X. Guan, Z. Yang, M. Zhou, et al., Small Struct. 3 (2022) 2200102.
[115] H. Chao, H. Qin, M. Zhang, et al., Adv. Funct. Mater. 31 (2021) 2007636.
[116] L. Zong, H. Wu, H. Lin, Y. Chen, Nano Res. 11 (2018) 4149–4168.
[117] S. Zhou, C. Gu, Z. Li, et al., Appl. Surf. Sci. 498 (2019) 143889.
[118] J.J. Z.hu, A. Hemesh, J.J. Biendicho, et al., J. Colloid Interface Sci. 623 (2022) 947–961.
[119] G. Wang, S. Guo, Y. Wu, et al., Small 18 (2022) e2202087.
[120] H. Chao, Y. Li, Y. Lu, et al., Sci. China Mater. 65 (2022) 2958–2966.
[121] G.J. Leigh, J. Organomet. Chem. 689 (2004) 2733–2742.
[122] S. Yang, J. Huo, H. Song, X. Chen, Electrochim. Acta 53 (2008) 2238–2244.
[123] M. Lu, B. Xie, J. Kang, et al., Chem. Mater. 17 (2004) 402–408.
[124] C.R. Mayer, R. Thouvenot, T. Lalot, Chem. Mater. 12 (2000) 257–260.
[125] S.A. Alshehri, A. Al Yasari, F. Marken, J. Fielden, Macromolecules 53 (2020) 11120–11129.
[126] X. Zhang, Y. Li, Y. Li, S. Wang, X. Wang, ACS Appl. Nano Mater. 2 (2019) 6971–6981.
[127] J.N. Chang, M. Zhang, G.K. Gao, et al., Energ. Fuel. 34 (2020) 16968–16977.
[128] S.K. H.wang, S.J. Patil, N.R. Chodankar, Y.S. Huh, Y.K. Han, Chem. Eng. J. 427 (2022) 131854.
[129] W. Chen, L. Huang, J. Hu, et al., Phys. Chem. Chem. Phys. 16 (2014) 19668–19673.
[130] Y. Ji, J. Hu, L. Huang, et al., Chem. Eur. J. 21 (2015) 6469–6474.
[131] E. Yucelen, I. Lazic, E.G.T. Bosch, Sci. Rep. 8 (2018) 2676.
[132] H.J. Lee, W. Ho, Science 286 (1999) 1719–1722.
[133] X.Y. Yang, W.J. Li, Z.L. Tan, et al., J. Mater. Chem. A 8 (2020) 25316–25322.
[134] W. Niu, Y. Zhu, R. Wang, et al., ACS Appl. Mater. Interfaces 12 (2020) 30805–30814.
[135] N. Hanikel, X. Pei, S. Chheda, et al., Science 374 (2021) 454–459.
[136] L. Chen, W. Wang, J. Tian, et al., Nat. Commun. 12 (2021) 4556.
[137] X. Xiong, B.Y. Huang, J.H. Li, H.J. Xu, Carbon 44 (2006) 463–467.
[138] P.J. Bereciartua, A. Cantin, A. Corma, et al., Science 358 (2017) 1068–1071.
[139] S.V. Aradhya, M. Frei, M.S. Hybertsen, L. Venkataraman, Nat. Mater. 11 (2012) 872–876.
[140] N. Wang, Q. Sun, J. Yu, Adv. Mater. 31 (2019) e1803966.
[141] D. Kumar, A. Joshi, G. Singh, R.K. Sharma, Chem. Eng. J. 431 (2022) 134085.
[142] Y. Chai, W. Dai, G. Wu, N. Guan, L. Li, Acc. Chem. Res. 54 (2021) 2894–2904.
[143] M. Gutierrez, Y. Zhang, J.C. Tan, Chem. Rev. 122 (2022) 10438–10483.
[144] B. Ni, H. Gao, Matter 4 (2021) 763–765.
[145] V.K.A. Fernández, D.M. Fernandes, S.S. Balula, L.C. Silva, C. Freire, J. Mater. Chem. A 8 (2020) 13509–13521.
[146] S.W. Li, R.M. Gao, R.L. Zhang, J.S. Zhao, Fuel 184 (2016) 18–27.
[147] H.B. Wu, X.W.D. Lou, Sci. Adv. 3 (2017) 16.
[148] A.M. Mohamed, M. Ramadan, N. Ahmed, et al., J. Energy Storage 28 (2020) 101292.
[149] T. Wei, M. Zhang, P. Wu, et al., Nano Energy 34 (2017) 205–214.
[150] M. Zhang, A.M. Zhang, X.X. Wang, et al., J. Mater. Chem. A 6 (2018) 8735–8741.
[151] J.Q. Sha, X.Y. Yang, Y. Chen, et al., ACS Appl. Mater. Interfaces 10 (2018) 16660–16665.
[152] D. Cao, Q. Sha, J. Wang, et al., ACS Appl. Mater. Interfaces 14 (2022) 22186–22196.
[153] S. Mukhopadhyay, J. Debgupta, C. Singh, A. Kar, S.K. Das, Angew. Chem. Int. Ed. 57 (2018) 1918–1923.
[154] Z. Xie, X. Li, R. Li, et al., Nanoscale 12 (2020) 17113–17120.
[155] M. Varela, A.R. Lupini, K.V. Benthem, et al., Annu. Rev. Mater. Res. 35 (2005) 539–569.
[156] Y. Wang, Y. Shi, L. Pan, et al., Nano Lett. 15 (2015) 7736–7741.
[157] L. Voorhaar, R. Hoogenboom, Chem. Soc. Rev. 45 (2016) 4013–4031.
[158] L. Pan, G. Yu, D. Zhai, et al., Proc. Natl. Acad. Sci. U. S. A. 109 (2012) 9287–9292.
[159] Y. Shi, L. Peng, G. Yu, Nanoscale 7 (2015) 12796–12806.
[160] M. Wang, Y. Yu, M. Cui, et al., Electrochim. Acta 329 (2020) 135181.
[161] M. Haider, S. Uhlemann, E. Schwan, et al., Nature 392 (1998) 768–769.
[162] Y. Liu, J. Li, Q. Shen, et al., eScience 2 (2022) 10–31.
[163] Q. Shen, Y. Liu, L. Jiao, X. Qu, J. Chen, Energy Storage Mater 35 (2021) 400–430.
[164] A.S. Cherevan, S.P. Nandan, I. Roger, et al., Adv. Sci. 7 (2020) 1903511.
[165] C.C. Lin, C.T. Hsu, W. Liu, et al., ACS Appl. Mater. Interfaces 12 (2020) 40296–40309.
[166] M.Y. Zhao, Z.Y. Ji, Y.G. Zhang, et al., Electrochim. Acta 252 (2017) 350–361.
[167] L. Liu, J. Han, L. Xu, et al., Science 368 (2020) 850–856.
[168] D.A. Britz, A.N. Khlobystov, Chem. Soc. Rev. 35 (2006) 637–659.
[169] J.W. Jordan, J.M. Cameron, G.A. Lowe, et al., Angew. Chem. Int. Ed. 61 (2022) e202115619.
[170] Q. Sha, D. Cao, J. Wang, et al., Chem 28 (2022) e202201899.
[171] O. Dyck, S. Kim, S.V. Kalinin, S. Jesse, Appl. Phys. Lett. 111 (2017) 113104.
[172] Z. Dong, B. Li, H. Shang, et al., Aiche J. 67 (2021) e17281.
[173] W. Cong, P. Song, Y. Zhang, et al., J. Hazard. Mater. 437 (2022) 129327.
[174] M.J. Hulsey, V. Fung, X. Hou, J. Wu, N. Yan, Angew. Chem. Int. Ed. 61 (2022) e202208237.